

Nondetection Zone Analytics for Unintentional Islanding in a Distribution Grid Integrated With Distributed Energy Resources

Yan Li, *Student Member, IEEE*, Peng Zhang , *Senior Member, IEEE*, Wenyuan Li , *Life Fellow, IEEE*, Joseph N. Debs, David A. Ferrante , Donald J. Kane, Samuel N. Woolard, Roderick Kalbfleisch , Kenneth B. Bowes, and Andrew J. Kasznay, *Member, IEEE*

Abstract—Given the progressively deeper integration of distributed energy resources (DERs), evaluating the potential unintentional islanding hazards in distribution networks becomes increasingly important for distribution system planning and operations. In this paper, a rigorous theoretical analysis is used to devise a DER-driven nondetection zone (D^2 NDZ) method, which is then implemented through a data-driven learning-based approach. Test results indicate that D^2 NDZ can quickly and effectively estimate the nondetection zones for any given distribution feeders, while avoiding numerous and time-consuming electromagnetic transient simulations. D^2 NDZ software has been deployed in Eversource Energy, a major power utility company in the northeastern U.S. In practice, D^2 NDZ reduces utilities engineers' case study time from months to just a few minutes.

Index Terms—DER-driven non-detection zone, distribute energy resource, non-detection zone, unintentional islanding, IEEE Standard 1547.

NOMENCLATURE

P_{DER}	Active power injection from DER units
Q_{DER}	Reactive power injection from DER units
P_G, Q_G	Active and reactive power at substation
P_L, Q_L	Active and reactive load
ΔV	Voltage deviation after islanding
ΔR	Resistance change after islanding
$\mu = \Delta V/V$	Voltage deviation

Manuscript received November 22, 2017; revised March 13, 2018; accepted April 19, 2018. Date of publication April 26, 2018; date of current version December 14, 2018. This work was supported in part by the National Science Foundation under Grant 1647209 and in part by the Eversource Energy Center under Grant 6200980 and Grant 6200990. Paper no. TSTE-01062-2017. (Corresponding author: Peng Zhang.)

Y. Li and P. Zhang are with the Department of Electrical and Computer Engineering, University of Connecticut, Storrs, CT 06269 USA (e-mail: yan.7.li@uconn.edu; peng.zhang@uconn.edu).

W. Li is with the State Key Laboratory of Power Transmission Equipment and System Security and New Technology, Chongqing University, Chongqing 400030, China (e-mail: wenyuan.li@ieee.org).

J. N. Debs, D. A. Ferrante, D. J. Kane, S. N. Woolard, R. Kalbfleisch, and K. B. Bowes are with Eversource Energy, Berlin, CT 06037 USA (e-mail: joseph.debs@eversource.com; david.ferrante@eversource.com; donald.kane@eversource.com; samuel.woolard@eversource.com; roderick.kalbfleisch@eversource.com; kenneth.bowes@eversource.com).

A. J. Kasznay was with Eversource Energy, Berlin, CT 06037 USA. He is now with the United Illuminating Company, New Haven, CT 06506 USA (e-mail: andrew.kasznay@uinet.com).

Color versions of one or more of the figures in this paper are available online at <http://ieeexplore.ieee.org>.

Digital Object Identifier 10.1109/TSTE.2018.2830748

$\rho = \Delta f/f$	Frequency deviation
N_{PV}	Number of PV units
N_{Ind}	Number of induction generators
N_{Syn}	Number of synchronous generators
N_{Bat}	Number of batteries
N_S	Number of experimental scenarios

I. INTRODUCTION

POWER distribution grids in the U.S. are being impacted by the increasingly deep integration of distributed energy sources (DERs) [1], [2]. For instance, as of 2016, there were 1.7 gigawatts of grid-tied DERs within Eversource Energy's service territory (Connecticut, Massachusetts, and New Hampshire), including over 12,000 residential solar photovoltaic (PV) projects installed in Connecticut and over 4,600 additional projects in progress, as shown in Fig. 1. This number is projected to be quadrupled within the next four years. Nationwide, a new PV was interconnected to the distribution grids every two minutes in 2015, a speed that is likely to increase in the future due to the significant drop in PV costs. Consequently, a major challenge that utility companies face is the possibility of unintentional islanding of a feeder, which can create safety hazards for utility customers and field crews [3]. Unintentional islanding is of particular concern when larger DERs are connected to a feeder, as such configurations may mimic normal grid conditions, causing the PV inverters' anti-islanding algorithms to be deceived into staying online and creating an unintentional island. This challenge rapidly escalates with the trend of more frequent storm-induced blackouts where DER units may continue to energize a power line from customers' homes or businesses.

To mitigate the detrimental impact without knowing the possibility of unintentional islanding, utility companies face prohibitively costly upgrades to install a new protection and communication infrastructure such as transfer trip facilities [4]. Furthermore, those expensive 'fit and forget' solutions can hardly accommodate the fast changes in DERs' plug-in, loads, and distribution grids. Another utility concern is that the UL 1741 unintentional islanding test is conducted on a single inverter at a time and does not address inverter or generation diversity on the distribution system. Therefore, it is unclear whether a deeper integration of DERs would increase the possibility that

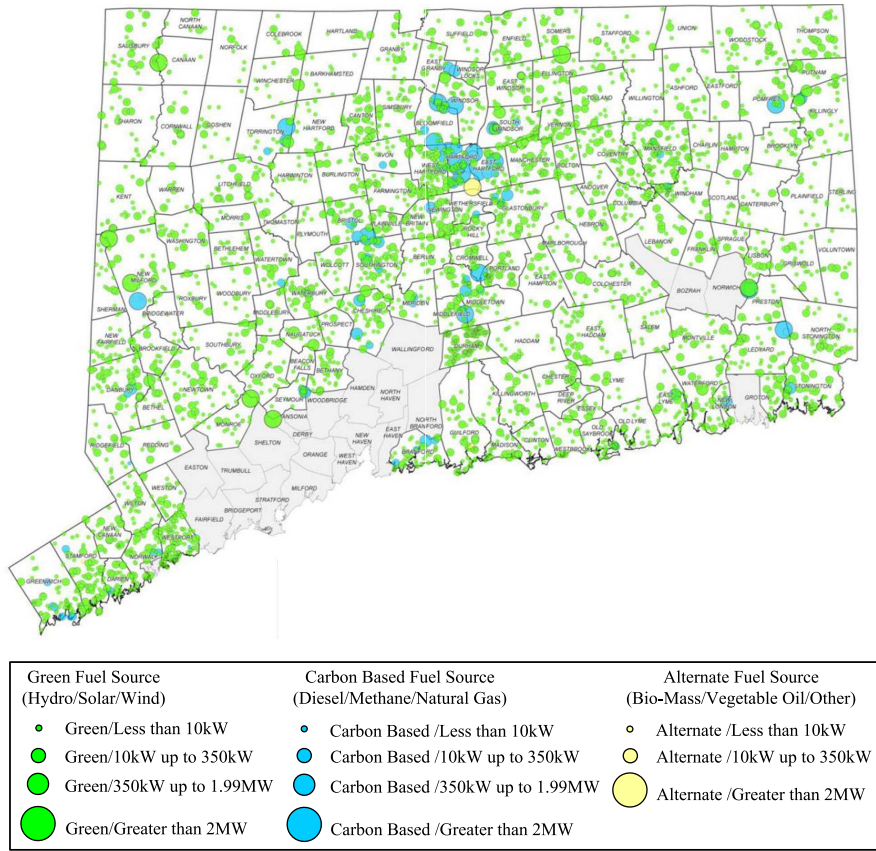


Fig. 1. DERs installed across Eversource service territory in Connecticut as of 2016.

unintentional island might not be detected or decrease? Thus, a pressing question to be addressed for distribution planning and operations is how to reliably assess unintentional islanding hazards of an arbitrary feeder in cases of high penetration scenarios.

Non-detection zone (NDZ) refers to the regions in an appropriately defined space where islanding detection schemes fail to detect the abnormal islanding mode [5]–[9]. Therefore, NDZ can serve as a practical metric for assessing the hazard of unintentional islanding. NDZ is often a by-product of anti-islanding methods which can be found in a plethora of literature falling into two main categories: active detection and passive detection. Active approaches, e.g., slip-mode frequency shift [10], active frequency drift [11], Sandia frequency shift [12], voltage shift [13], high frequency signal injection [14], positive-feed-back-based method [15], d-axis disturbance signal injection [16], and reactive power disturbance [17], have fast responses while causing perturbations in the distribution systems. Passive approaches, e.g., Bayesian passive method [18], rate of change of frequency [19], over/under frequency [19], over/under voltage [19], fuzzy method [20], pattern recognition [21], and phase jump detection [22], do not disturb the system while generating a more conservative NDZ than active methods. Examining NDZ under the deep integration of DERs in large distribution grids, however, remains an open challenge.

Motivated by the challenges detailed above, a learning-based, DER-driven non-detection zone (D^2 NDZ) evaluation method is devised to effectively quantify the NDZs in distribution networks with the deep integration of DERs. Our main contributions are three-fold:

- D^2 NDZ incorporates both the steady-state and dynamic impacts of different types of DER units. Particularly, a series of formulas are derived to compute the contribution of the dynamic characteristics of various DERs to NDZ, making the D^2 NDZ results extremely close to those obtained from detailed simulation-based methods.
- D^2 NDZ establishes an optimization-based learning scheme that estimates NDZs for any grids quickly and effectively without precise electromagnetic transients simulations, which offers an ultra-fast means of evaluating a system's islanding possibilities.
- A D^2 NDZ software tool has been developed and successfully implemented for operational planning in Eversource Energy, the largest power utility company in the Northeast.

The remainder of this paper is organized as follows: Section II establishes the methodological foundations for this study, and Section III discusses how D^2 NDZ's learning parameters were formulated as an optimization problem. Section IV presents the implementation of D^2 NDZ. In Section V, tests on Eversource Energy's distribution feeders verify the effectiveness and scalability of D^2 NDZ. Conclusions are drawn in Section VI.

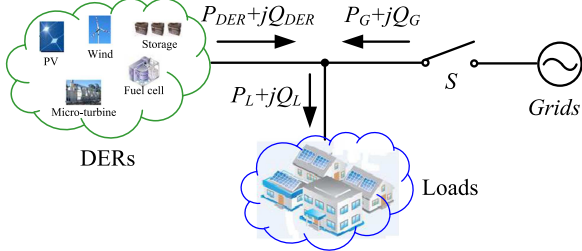


Fig. 2. A schematic distribution feeder showing aggregated load and DER.

II. ANALYTICAL METHOD OF D²NDZ

Mathematically, the boundary of NDZ is a hull made up of critical operating points. Based on the research results in [7], the generation to load ratio (G/L) and the power factor are good candidates that can be selected to form a two-dimensional NDZ. For a distribution feeder with a deep integration of DERs (see Fig. 2 [7]), its NDZ is determined by the total effect of both steady state and dynamic behaviors of loads and DERs after the feeder is disconnected from the main grid [23]. Therefore, one can construct a baseline NDZ, that is determined by the steady state of the feeder and then augment it by incorporating the dynamic impacts of DERs. This forms the basic idea of our D²NDZ approach. The constructed NDZ can thus be expressed as

$$\left[\frac{P_{DER}}{P_L}, \frac{\overline{P}_{DER}}{P_L} \right] = \quad (1)$$

$$\left[\left(\frac{P_{DER}}{P_L} \right)_S + \left(\frac{P_{DER}}{P_L} \right)_D, \left(\overline{\frac{P_{DER}}{P_L}} \right)_S + \left(\overline{\frac{P_{DER}}{P_L}} \right)_D \right],$$

$$\left[\frac{Q_G}{P_L}, \frac{\overline{Q}_G}{P_L} \right]$$

$$= \left[\left(\frac{Q_G}{P_L} \right)_S + \left(\frac{Q_G}{P_L} \right)_D, \left(\overline{\frac{Q_G}{P_L}} \right)_S + \left(\overline{\frac{Q_G}{P_L}} \right)_D \right], \quad (2)$$

where $\left(\frac{P_{DER}}{P_L} \right)_S$, $\left(\overline{\frac{P_{DER}}{P_L}} \right)_S$ represent the lower and upper bounds of G/L when only the steady state is considered; $\left(\frac{Q_G}{P_L} \right)_S$, $\left(\overline{\frac{Q_G}{P_L}} \right)_S$ represent the lower and upper bounds of the power factor when only the steady state is considered; $\left(\frac{P_{DER}}{P_L} \right)_D$, $\left(\overline{\frac{P_{DER}}{P_L}} \right)_D$ represent the impacts of DER dynamics on lower and upper bounds of G/L; $\left(\frac{Q_G}{P_L} \right)_D$, $\left(\overline{\frac{Q_G}{P_L}} \right)_D$ represent the impacts of DER dynamics on the lower and upper bounds of the power factor. Our task, therefore, is to identify such a zone well approximating the actual NDZ.

A. Derivation of Baseline Nondetection Zone

1) *G/L Bounds*: Islanding detection normally takes only a few cycles, whereas DER units such as PV array and wind turbine generators usually operate at maximum power points that do not change instantaneously. This means that DER power outputs can be treated as constants when the steady-state is analyzed [17]. Therefore, the active power consumption along

the feeder before and after islanding (circuit breaker S tripped off and switched on) can be expressed by (3) and (4), respectively [7].

$$P_L = P_{DER} + P_G = \frac{V^2}{R}, \quad (3)$$

$$P_{DER} = \frac{(V + \Delta V)^2}{R + \Delta R}, \quad (4)$$

where the expanded form of ΔR can be found in Appendix I. As a result, the G/L ratio due to steady-state conditions can be expressed as

$$\left(\frac{P_{DER}}{P_L} \right)_S = \frac{(V + \Delta V)^2}{V^2} \cdot \frac{R}{R + \Delta R} = (1 + \mu)^2 \cdot \frac{1}{1 + \frac{\Delta R}{R}}. \quad (5)$$

Based on Appendix I,

$$\frac{\Delta R}{R} = \frac{\Delta R_P + \Delta R_C}{R_I + R_P + R_C} = \frac{(2\mu + \mu^2)P_I P_C + \mu P_I P_P}{P_I P_C + P_I P_P + P_P P_C}, \quad (6)$$

where P_I , P_P , P_C are the percentages of constant impedance, constant power and constant current loads, respectively. Substituting (6) into (5), G/L can be rewritten as

$$\left(\frac{P_{DER}}{P_L} \right)_S = \frac{(1 + \mu)^2(P_I P_C + P_I P_P + P_P P_C)}{(1 + \mu)^2 P_I P_C + (1 + \mu)P_I P_P + P_P P_C} = f(\mu, P_I, P_P, P_C). \quad (7)$$

Consequently, by considering the voltage deviation bounds within which an island may not be detected, the G/L bounds $\left(\frac{P_{DER}}{P_L} \right)_S$ and $\overline{\left(\frac{P_{DER}}{P_L} \right)_S}$ can be evaluated by

$$\left(\frac{P_{DER}}{P_L} \right)_S = \min f(\mu, P_I, P_P, P_C), \quad (8)$$

$$\overline{\left(\frac{P_{DER}}{P_L} \right)_S} = \max f(\mu, P_I, P_P, P_C), \quad (9)$$

where μ means voltage deviations under different islanding durations with typical values given in Section V.

2) *Power Factor Bounds*: The reactive power consumed in the feeder load before and after islanding can be formulated in (10) and (11), respectively.

$$Q_L = Q_{DER} + Q_G = V^2 \left(\frac{1}{2\pi f L} - 2\pi f C \right), \quad (10)$$

$$Q_{DER} = (V + \Delta V)^2 \left(\frac{1}{2\pi(f + \Delta f)(L + \Delta L)} - 2\pi(f + \Delta f)(C + \Delta C) \right). \quad (11)$$

Thus, the power factor can be calculated by [7]

$$\left(\frac{Q_G}{P_L} \right)_S = R \left(\frac{1}{2\pi f L} - 2\pi f C \right) - (1 + \mu)^2 R \cdot \left(\frac{1}{2\pi(f + \Delta f)(L + \Delta L)} - 2\pi(f + \Delta f)(C + \Delta C) \right). \quad (12)$$

By defining the quality factor $Q_f = \frac{R}{2\pi f L} = 2\pi f RC$, (12) can be re-formulated as [7]

$$\left(\frac{Q_G}{P_L}\right)_S = (1+\mu)^2(1+\rho)Q_f \left(\frac{\Delta L}{L} + \frac{\Delta C}{C}\right). \quad (13)$$

Note that, (14) and (15) have been substituted in (12) to derive (13). (14) and (15) are justified because the variations in load inductance and capacitance are small before and after islanding [7].

$$\Delta L \cdot \Delta C \approx 0, \quad (14)$$

$$1 + \frac{\Delta L}{L} \approx 1. \quad (15)$$

According to the relationship of the load resonant frequency before and after islanding (see Appendix III), $\frac{\Delta L}{L} + \frac{\Delta C}{C}$ can be expressed as,

$$\frac{\Delta L}{L} + \frac{\Delta C}{C} = \frac{1}{(1+\rho)^2} - 1. \quad (16)$$

Substituting (16) into (13), the power factor can be rewritten as follows:

$$\left(\frac{Q_G}{P_L}\right)_S = (1+\mu)^2(1+\rho)Q_f \left(\frac{1}{(1+\rho)^2} - 1\right) = g(\mu, \rho, Q_f). \quad (17)$$

Consequently, by considering the voltage and frequency deviation bounds within which an island may not be detected, the power factor bounds $\underline{\left(\frac{Q_G}{P_L}\right)_S}$ and $\overline{\left(\frac{Q_G}{P_L}\right)_S}$ can be obtained by

$$\underline{\left(\frac{Q_G}{P_L}\right)_S} = \min g(\mu, \rho, Q_f), \quad (18)$$

$$\overline{\left(\frac{Q_G}{P_L}\right)_S} = \max g(\mu, \rho, Q_f), \quad (19)$$

where ρ means frequency deviations under different islanding durations with typical values given in Section V.

B. Nondetection Zone Bounds Driven by DER Dynamics

Besides the steady-state behaviors, the transient processes of the DER units also significantly impact NDZ, especially on its boundary. In order to incorporate this effect, detailed DER models are built at the beginning [24], [25]; and scenarios in various distribution feeders are then tested via electromagnetic transient (EMT) simulations to provide experimental data; finally, these experimental data are analyzed and learned to develop a generic formulation which is used to augment the baseline NDZ. Considering the deep integration of PVs, small hydro units (induction generator or synchronous generator), and battery storages in Eversource Energy, these types of DER units are analyzed in detail. Other types of DERs can be models in the D²NDZ study following the same procedure.

1) *Impact of DER Dynamics on G/L Bounds:* Our experimental results obtained from EMT simulations show that the impact of DER dynamics on NDZ bounds is strongly related to the number of the connected DERs, i.e., the more power

electronics interfaced non-dispatchable DERs (e.g., PV) a system has, the more compact its NDZ will be. This seemingly counter-intuitive phenomenon can be explained as follows: The control systems of DERs must be properly coordinated to enable a seamless transition from the grid-connected mode to the islanded mode [24]. In practice, it is very difficult to achieve this goal when multiple DERs are integrated at different locations without communication, exponentially reducing the size of NDZ. Therefore, exponential models are established to reflect the impact of DER dynamics on NDZ bounds. The following exponential model is given as an example to characterize the impact of PV dynamics on G/L bounds.

$$\phi_{PV,L} = \beta_{PV,L} (1 - \alpha_{PV,L} e^{-N_{PV}}), \quad (20)$$

$$\phi_{PV,H} = \beta_{PV,H} (1 - \alpha_{PV,H} e^{-N_{PV}}), \quad (21)$$

where $e^{(\cdot)}$ means the exponential function; coefficients $\beta_{PV,L}, \alpha_{PV,L}, \beta_{PV,H}, \alpha_{PV,H}$ can be determined by learning the experimental data. Note that, after data learning, $\beta_{PV,L}$ and $\beta_{PV,H}$ should be updated by multiplying a coefficient to ensure a conservative NDZ estimation. Likewise, the impacts of induction generators, synchronous generators, battery storage, or any other type of DER can be respectively modeled as follows:

$$\phi_{Ind,L} = \beta_{Ind,L} (1 - \alpha_{Ind,L} e^{-N_{Ind}}), \quad (22)$$

$$\phi_{Ind,H} = \beta_{Ind,H} (1 - \alpha_{Ind,H} e^{-N_{Ind}}), \quad (23)$$

$$\phi_{Syn,L} = \beta_{Syn,L} (1 - \alpha_{Syn,L} e^{-N_{Syn}}), \quad (24)$$

$$\phi_{Syn,H} = \beta_{Syn,H} (1 - \alpha_{Syn,H} e^{-N_{Syn}}), \quad (25)$$

$$\phi_{Bat,L} = \beta_{Bat,L} (1 - \alpha_{Bat,L} e^{-N_{Bat}}), \quad (26)$$

$$\phi_{Bat,H} = \beta_{Bat,H} (1 - \alpha_{Bat,H} e^{-N_{Bat}}), \quad (27)$$

where, $\phi_{Ind,L}$ and $\phi_{Ind,H}$ characterize the impact of induction generators' dynamics on G/L bounds, $\phi_{Syn,L}$ and $\phi_{Syn,H}$ characterize the impact of synchronous generators' dynamics on G/L bounds, $\phi_{Bat,L}$ and $\phi_{Bat,H}$ characterize the impact of battery storage's dynamics on G/L bounds.

Subsequently, the overall impact of DER dynamics on the lower and upper bounds of G/L (G/L being the first dimension of NDZ) can be expressed as a weighted sum of individual contributions from different types of DERs. For instance, if PV, induction generator, synchronous generator and battery storage are considered, the overall effect of DER dynamics on G/L bounds can be expressed as:

$$\left(\frac{P_{DER}}{P_L}\right)_D = \delta_{PV} \phi_{PV,L} - \delta_{Ind} \phi_{Ind,L} - \delta_{Syn} \phi_{Syn,L} - \delta_{Bat} \phi_{Bat,L}, \quad (28)$$

$$\left(\frac{P_{DER}}{P_L}\right)_D = -\delta_{PV} \phi_{PV,H} + \delta_{Ind} \phi_{Ind,H} + \delta_{Syn} \phi_{Syn,H} + \delta_{Bat} \phi_{Bat,H}, \quad (29)$$

where $\delta_{PV}, \delta_{Ind}, \delta_{Syn}, \delta_{Bat}$ are Kronecker signs.

2) *Impact of DER Dynamics on Power Factor Bounds:* Similar to the analysis above, the overall impact of DER dynamics

on the lower and upper bounds of the power factor, which represents the second dimension of NDZ, can be presented by a weighted sum of the contributions from each type of DERs, as shown below.

$$\left(\frac{Q_G}{P_L} \right)_D = \delta_{PV} \varphi_{PV,L} - \delta_{Ind} \varphi_{Ind,L} - \delta_{Syn} \varphi_{Syn,L} - \delta_{Bat} \varphi_{Bat,L}, \quad (30)$$

$$\left(\frac{Q_G}{P_L} \right)_D = -\delta_{PV} \varphi_{PV,H} + \delta_{Ind} \varphi_{Ind,H} + \delta_{Syn} \varphi_{Syn,H} + \delta_{Bat} \varphi_{Bat,H}, \quad (31)$$

where the contributing factors are given by:

$$\varphi_{PV,L} = \gamma_{PV,L} (1 - \eta_{PV,L} e^{-N_{PV}}), \quad (32)$$

$$\varphi_{PV,H} = \gamma_{PV,H} (1 - \eta_{PV,H} e^{-N_{PV}}), \quad (33)$$

$$\varphi_{Ind,L} = \gamma_{Ind,L} (1 - \eta_{Ind,L} e^{-N_{Ind}}), \quad (34)$$

$$\varphi_{Ind,H} = \gamma_{Ind,H} (1 - \eta_{Ind,H} e^{-N_{Ind}}), \quad (35)$$

$$\varphi_{Syn,L} = \gamma_{Syn,L} (1 - \eta_{Syn,L} e^{-N_{Syn}}), \quad (36)$$

$$\varphi_{Syn,H} = \gamma_{Syn,H} (1 - \eta_{Syn,H} e^{-N_{Syn}}), \quad (37)$$

$$\varphi_{Bat,L} = \gamma_{Bat,L} (1 - \eta_{Bat,L} e^{-N_{Bat}}), \quad (38)$$

$$\varphi_{Bat,H} = \gamma_{Bat,H} (1 - \eta_{Bat,H} e^{-N_{Bat}}), \quad (39)$$

where, $\varphi_{PV,L}$ and $\varphi_{PV,H}$ characterize the impact of PV's dynamics on power factor bounds, $\varphi_{Ind,L}$ and $\varphi_{Ind,H}$ characterize the impact of induction generators' dynamics on power factor bounds, $\varphi_{Syn,L}$ and $\varphi_{Syn,H}$ characterize the impact of synchronous generators' dynamics on power factor bounds, $\varphi_{Bat,L}$ and $\varphi_{Bat,H}$ characterize the impact of battery storage's dynamics on power factor bounds.

III. PARAMETER OPTIMIZATION IN D²NDZ

As an estimation method, the performance of D²NDZ mainly depends on the parameters in each formula, e.g., $\alpha_{PV,L}$, $\alpha_{PV,H}$, etc. In this paper, an optimization-based learning approach is developed to determine these parameters from the experiments' data. This will guarantee that the formulas learned will produce NDZs as close as possible to those provided by electromagnet transients simulations that are often prohibitively expensive in practice. A salient feature of this parameter determination method is its capability to adapt to new information, which means it can use online or offline learning to update parameters, making D²NDZ more accurate over a longer period of time.

The parameter determination of D²NDZ are formulated into four independent optimization problems in that the parameters for identifying any of the four bounds of NDZ are independent of those for the other bounds. For instance, (40) shows the optimization formulation for learning the parameters that determine the lower bound of G/L. Here $\left(\frac{P_{DER}}{P_L} \right)_i^E$ is the exact lower bound of G/L in the i th experiment, $\left(\frac{P_{DER}}{P_L} \right)_i$ is the estimated lower bound of G/L from D²NDZ, and X denotes

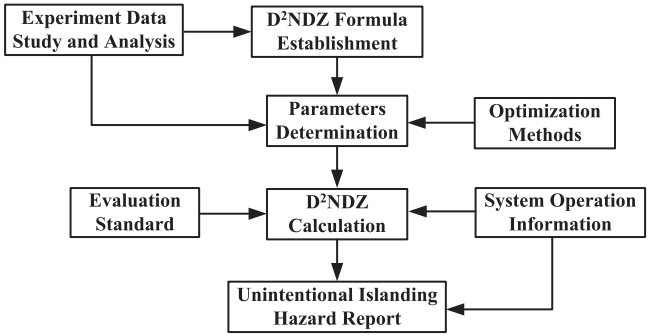


Fig. 3. Flowchart of D²NDZ computations.

the set of the parameters to be determined, i.e., $\beta_{PV,L}$, $\alpha_{PV,L}$, $\beta_{Ind,L}$, $\alpha_{Ind,L}$, $\beta_{Syn,L}$, $\alpha_{Syn,L}$, $\beta_{Bat,L}$, and $\alpha_{Bat,L}$. Note that the experimental data can be classified into different groups if necessary [26]. One D²NDZ can be established in each group to estimate their NDZs with a relatively high precision.

$$\begin{cases} \min f = \sum_{i=1}^{N_S} m_i \left(\left(\frac{P_{DER}}{P_L} \right)_i^E (X) - \left(\frac{P_{DER}}{P_L} \right)_i \right)^2 \\ \text{s.t. } X \in \mathbb{R}^n. \end{cases} \quad (40)$$

In (40), N_S ($\gg 1$) experimental scenarios are generated on the test systems to improve the robustness of D²NDZ. The weight coefficient m_i of a scenario should be increased if the probability of the i th operation scenario increases [24].

IV. IMPLEMENTATION OF D²NDZ

The procedures of D²NDZ, including NDZ estimation and unintentional islanding evaluation, are summarized in a flowchart shown in Fig. 3.

In Fig. 3, D²NDZ Formulas are initially established based on *Experiment Data Study and Analysis*. Parameters involved in these formulas are then determined through optimization methods. Then D²NDZ Calculation will be carried out based on the *Evaluation Standard* and the actual *Operation Information* of a system, e.g., numbers of DER units, power load, etc. Meanwhile, the unintentional islanding hazards can be assessed and reported by using the system's actual *Operation Information*, which will be discussed in Section V. Note that experiment data which needs special arrangement and time for preparation is essential to the parameter learning process of D²NDZ (see Section III). Further studies can be performed to improve the parameter learning process if necessary [26], [27].

A software tool with an easy-to-use Excel interface has been developed and deployed in Eversource Energy for the planning and operation of DER interconnections. In the future, experiment database and system operation information can be updated online which will enable D²NDZ to serve as a real-time tool for running unintentional islanding analytics.

V. TEST AND VALIDATION OF D²NDZ

A distribution feeder in Eversource Energy which consists of 3717 sections, three PV arrays, and one induction generator based hydro power station is used to validate D²NDZ. Since

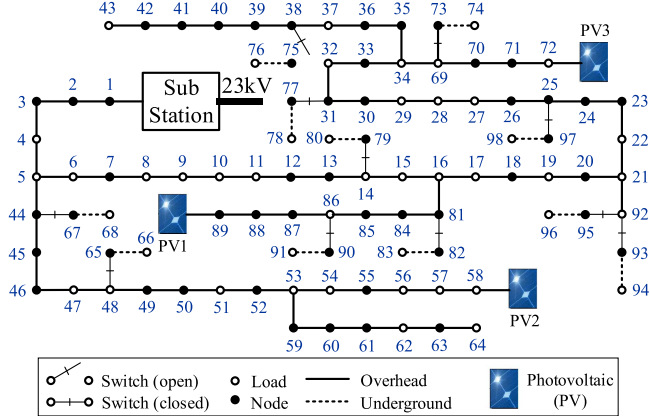


Fig. 4. A typical distribution feeder in Eversource Energy.

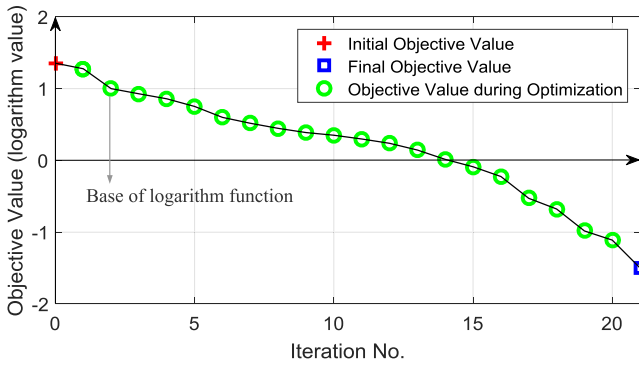


Fig. 5. Objective function value during the parameter optimization process.

the topology of an actual distribution grid is very complex, reasonable system reduction is necessary to accelerate system modeling, simulation and evaluation. Fig. 4 shows schematic one-line diagram of the equivalent feeder, with more details given in Appendix IV. The high-fidelity of the reduced model in re-producing system dynamics and steady state behaviors has been thoroughly validated [28], which is omitted due to limited space. Note that the D²NDZ approach is also potentially applied to a distribution feeder with the mesh topology.

A. Learning Parameters

As the flowchart in Fig. 3 demonstrates, it is fundamentally important to generate experiment data for D²NDZ to learn coefficients. Based on IEEE Standard 1547 [29], three critical islanding durations, i.e., 1 s, 2 s, 3 s, have been studied. Where 1 s means the islanding situation can last for at least 1 s with voltage and frequency in acceptable ranges; 2 s means the islanding situation can last for at least 2 s; and 3 s means the islanding situation will last for more than 3 s, which is the most dangerous case for utilities, because both voltage and frequency are within normal operation ranges in these scenarios; and thus, unintentional islanding cannot be detected.

Note that the NDZ corresponding to each islanding duration is formulated as four optimization problems, as shown in (40). Fig. 5 depicts the change in the objective function in optimizing (40) to determine X , which validates the effectiveness of the pa-

TABLE I
TYPICAL RANGES ADOPTED BY EVERSOURCE ENERGY

Durations	μ_{min}	μ_{max}	ρ_{min}	ρ_{max}
$\geq 1s$	-0.5000	0.2000	-0.0083	0.0667
$\geq 2s$	-0.5000	0.1000	-0.0083	0.0333
$\geq 3s$	-0.1200	0.1000	-0.0083	0.00085

TABLE II
OPTIMIZATION RESULTS FOR D²NDZ COEFFICIENTS

Durations	$\alpha_{PV,L}$	$\alpha_{PV,H}$	$\alpha_{Ind,L}$	$\alpha_{Ind,H}$	$\alpha_{Syn,L}$	$\alpha_{Syn,H}$
$\geq 1s$	0.4803	0.3215	1.4127	1.9704	1.8803	1.8128
$\geq 2s$	0.3601	0.4125	1.6402	2.4150	2.0549	1.7842
$\geq 3s$	1.0802	0.3549	1.5921	2.0543	1.8845	1.8123
Durations	$\eta_{PV,L}$	$\eta_{PV,H}$	$\eta_{Ind,L}$	$\eta_{Ind,H}$	$\eta_{Syn,L}$	$\eta_{Syn,H}$
$\geq 1s$	0.1583	0.2060	0.2596	0.1368	0.2037	0.1905
$\geq 2s$	0.1548	0.0195	0.0861	0.1345	0.1950	0.2306
$\geq 3s$	0.1105	0.0201	0.1008	0.1435	0.1503	0.1809
Durations	$\alpha_{Bat,L}$	$\alpha_{Bat,H}$	$\eta_{Bat,L}$	$\eta_{Bat,H}$		
$\geq 1s$	1.8028	1.6813	0.2810	0.1692		
$\geq 2s$	1.8835	1.7421	0.1460	0.1816		
$\geq 3s$	1.8320	1.6902	0.1205	0.1712		

TABLE III
ERRORS OF FOUR NDZ BOUNDARIES IN EACH CASE

Errors	Case 1			Case 2		
	(a)	(b)	(c)	(d)	(e)	(f)
$e_{x\min}$	0.78%	2.05%	0.99%	1.54%	1.64%	3.09%
$e_{x\max}$	1.91%	0.03%	0.48%	0.51%	0.16%	2.70%
$e_{y\min}$	0.03	0.02	0.07	0.02	0.01	0.006
$e_{y\max}$	0.05	0.11	0.04	0.01	0.006	0.003

rameters learning in D²NDZ. For a better illustration, logarithm values are adopted for the y axis, with the objective value at iteration 2 being selected as the base of the logarithm function. Table I summarizes the typical modified ranges correlated to IEEE Standard 1547, which are adopted by Eversource Energy in practice, and Table II shows the D²NDZ coefficients obtained from parameters optimization.

B. Verification of NDZ Analytics

1) *Comparisons Between D²NDZ and Simulation-Based Method:* Comparisons of NDZs constructed by D²NDZ and EMT simulations are shown in Fig. 6, where two cases are given as examples. In Case 1, only PV1 is integrated in the test feeder, whereas all three PV arrays are interconnected in Case 2. In both cases, the load percentages are set as: $P_L = 0$, $P_P = 50\%$, $P_C = 50\%$. In each case, the errors in the four NDZ bounds for three different islanding durations are calculated via the following assessment indices, as summarized in Table II. The errors are consistently small, which verifies the accuracy of D²NDZ.

$$e_{x\min} = \left| \left(\frac{P_{DER}}{P_L} \right) \bigg/ \left(\frac{P_{DER}}{P_L} \right)^{EMT} - 1 \right| \times 100\%, \quad (41)$$

$$e_{x\max} = \left| \overline{\left(\frac{P_{DER}}{P_L} \right)} \bigg/ \left(\frac{P_{DER}}{P_L} \right)^{EMT} - 1 \right| \times 100\%, \quad (42)$$

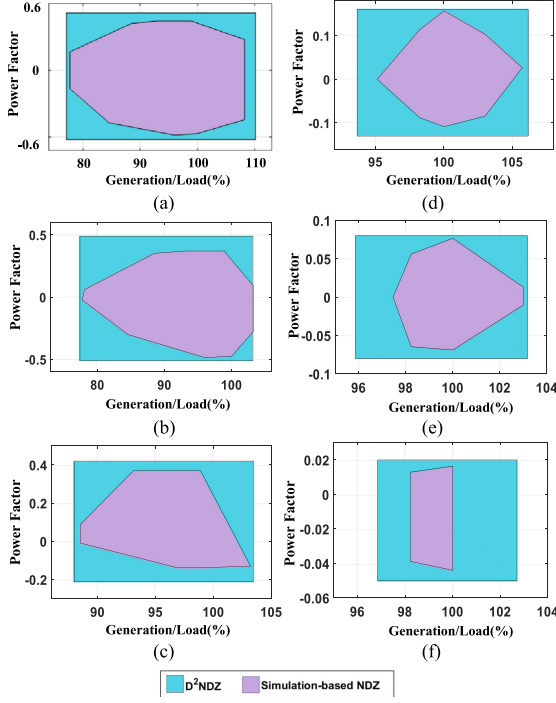


Fig. 6. Comparisons between D²NDZ and simulation-based method. (a) 1s NDZ Comparison in case 1. (b) 2s NDZ Comparison in case 1. (c) 3s NDZ Comparison in case 1. (d) 1s NDZ Comparison in case 2. (e) 2s NDZ Comparison in case 2. (f) 3s NDZ Comparison in case 2.

$$e_{y \min} = \left| \left(\frac{Q_G}{P_L} \right) \left/ \left(\frac{Q_G}{P_L} \right)^{EMT} - 1 \right|, \quad (43)$$

$$e_{y \max} = \left| \left(\frac{Q_G}{P_L} \right) \left/ \left(\frac{Q_G}{P_L} \right)^{EMT} - 1 \right|, \quad (44)$$

Fig. 6 offers the following insights:

- NDZs obtained from D²NDZ closely approach those from the EMT simulations within acceptable errors, meaning D²NDZ is *effective*;
- Through the learned formulas, D²NDZ can quickly estimate NDZs for any given feeder [28] without numerous and time consuming EMT simulations, meaning D²NDZ is *efficient*;
- An NDZ constructed by D²NDZ always over-approximates the irregular NDZ obtained from point by point EMT simulations, meaning D²NDZ is *dependable*. This feature, in fact, is extremely important and helpful in practice, since it gives an early warning to utility engineers in advance when a feeder's operating point is approaching NDZ.

The EMT simulation results in two cases are also compared in Fig. 7 to verify that the more power electronics interfaced non-dispatchable DERs a system has, the more compact the NDZ will be.

2) *Impacts of DER Units on NDZ*: The progressively deeper integration of DERs, especially power electronics interfaced units (e.g., PV and battery), is significantly changing distribution grids' transient performance. Therefore, it is critically important to explore the impact of different DER units on NDZ. Fig. 8

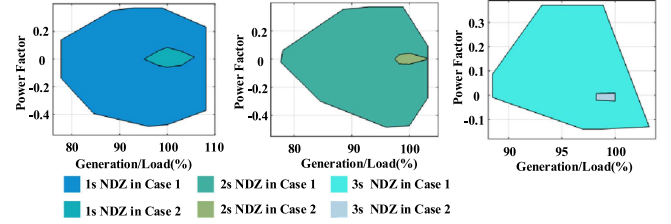


Fig. 7. Comparisons of NDZ in two cases.

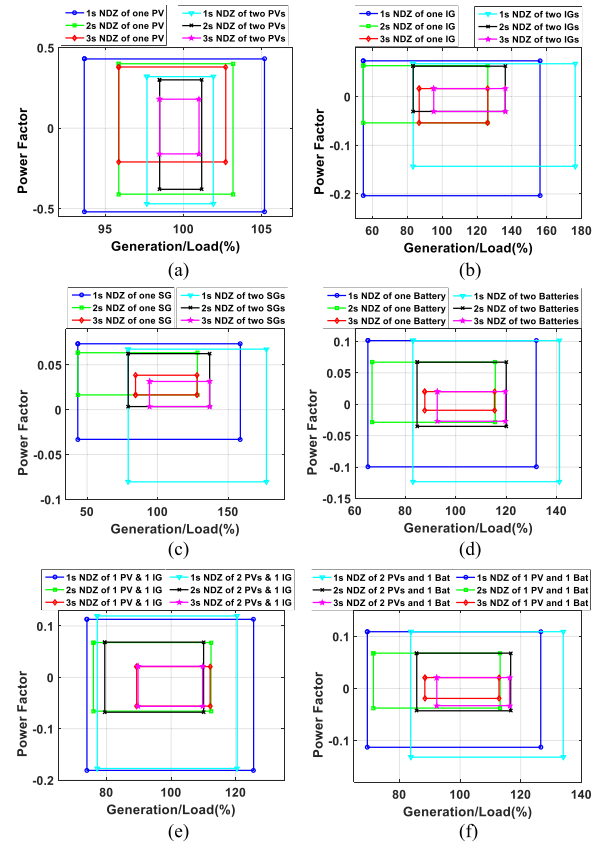


Fig. 8. Impacts of DER units on NDZ. (a) Impacts of PV on NDZ. (b) Impacts of induction generator on NDZ. (c) Impacts of synchronous generator on NDZ. (d) Impacts of battery on NDZ. (e) Impacts of combination of PV and induction generator on NDZ. (f) Impacts of combination of PV and battery on NDZ.

shows the D²NDZ results for six different cases where the only difference is the combination of DERs while the feeder configuration and loading conditions remain the same. The load percentages in each case are set as $P_I = 0$, $P_P = 50\%$, $P_C = 50\%$. The following can be observed:

- *Impact of Conventional Generators on D²NDZ Boundary*: The interconnection of induction (or synchronous) generators are able to enlarge the boundary of NDZ, as shown in Fig. 8(b) and (c).

The reason is that both induction and synchronous generators are rotating machines providing considerable inertia. In addition, some generators are equipped with exciter and governor controllers which enable them to ride-through transient processes. With these machines, it is likely a distribution feeder can survive as an island with acceptable

voltages and frequency for a few seconds or longer, creating much larger NDZs for 1 s, 2 s, and 3 s.

- *Impact of Power Electronics on Baseline NDZ:* Power electronics interfaces decrease the baseline boundaries of NDZ, which is obtained when only the steady-state is considered (using (7) and (17)). For instance, the baseline NDZ for the case 3 s NDZ of one PV in Fig. 8(a) is [77.44%, 121%] for G/L and [−0.0502, 0.0506] for the power factor, which is significantly larger than the overall NDZ obtained by D²NDZ.

The reason is that low-inertia power electronic interfaces make the distribution feeder so sensitive to disturbances that their dramatic transient process can easily violate the volt/frequency requirements specified in IEEE Standard 1547 and thus can hardly sustain an island.

- *Impact of Power Electronics on D²NDZ Boundary:* Under deep DER integration, e.g., when G/L is around 100%, the more power-electronics-interfaced DER units a distribution feeder has, the smaller its NDZ would be, as shown in Fig. 8(a) and (b).

The reason is that the D²NDZ boundary is largely related to the DER transient process which is mainly determined by DER controllers. It is basically infeasible to coordinate design their control parameters so as to seamlessly switch a feeder to operate in islanded mode.

- *Impact of Battery on D²NDZ Boundary:* The NDZ of a feeder integrated with an inverter interfaced battery is larger than that of a feeder integrated with PV, but smaller than that of induction or synchronous generators, as shown in Fig. 8(d).

Although power-electronics-interface leads to a relatively smaller NDZ, as an energy storage device is usually controlled by a droop strategy [24], a grid-connected battery system can adjust its real and reactive power outputs and thus respond to the grid disturbances. Consequently, battery storage helps stabilize an isolated distribution feeder and results in a relatively larger NDZ than PV does.

- *Impact of PV on D²NDZ Boundary:* Fig. 8(e) and (f) show that the emergence of MPPT controlled PV [24] in a system brings about a smaller NDZ than the case when the system only has an induction generator or battery. Adding low-inertial DERs in the generation mix, therefore, decreases the NDZ boundaries.

3) *Impacts of Loads on NDZ:* NDZ results are also impacted by the percentages of a load mix, especially the baseline NDZ as shown in (7). Taking G/L as an example, it can be seen in Fig. 9 how the upper and lower bounds of the baseline G/L vary with the load percentages.

Fig. 9 offers the following insights:

- Different load compositions significantly change the lower and upper bounds of NDZ, indicating loads play an important role in forming an unintentional island.
- When $P_I = 0$, the lower bound of the baseline G/L reaches its minimum (25%); meanwhile, the corresponding upper bound is 144%, which is its maximum. Therefore, if a system has no constant impedance load, its baseline NDZ becomes very large. When $P_I = 63.01\%$, $P_P = 0.99\%$ and $P_C = 36.00\%$, the lower bound of base-

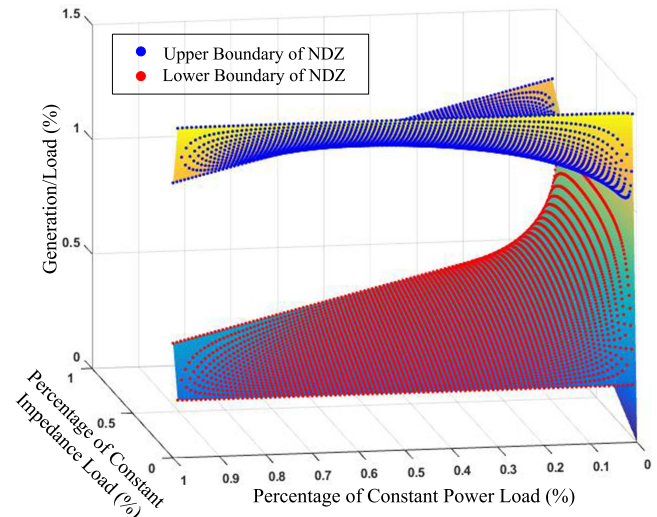


Fig. 9. Impacts of loads on baseline NDZ.

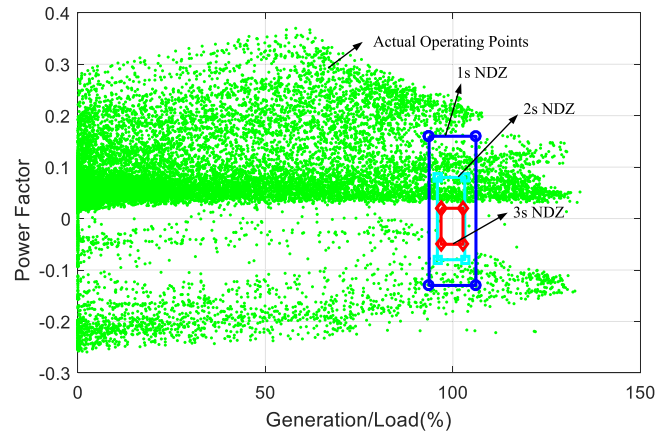


Fig. 10. Unintentional islanding frequencies assessment.

line G/L reaches its maximum (93.32%); meanwhile, the corresponding upper bound is 100.91%. When $P_I = 57.01\%$, $P_P = 0.99\%$, $P_C = 42.00\%$, the upper bound of the baseline G/L reaches its minimum (100.89%); meanwhile, the lower bound of G/L is 93.22%. Therefore, when a system has around a 60% constant impedance load and almost zero constant power load, its NDZ becomes very small.

C. Unintentional Islanding Frequencies

Once NDZs are obtained from D²NDZ, the unintentional islanding hazards of the test feeder can be approximately assessed by estimating the frequencies at which the operating points fall into the NDZs when the feeder is tripped off. The frequencies assessment for Case 1 in the above Subsection B (see Fig. 6) is illustrated in Fig. 10, where the sampling rate of the actual operating points is 15 minutes.

First we count the number of operating points (green dots in Fig. 10) that enter the NDZs and divide it by the total number of operating points over a specific time interval (normally one year). This probability multiplied by the probability of feeder tripping incidents gives the unintentional islanding probability.

Fig. 10 shows the conditional probability that operating points falling into 1 s, 2s, 3 s NDZs are 5.67%, 5.35%, and 2.44%, respectively. If the probability of feeder tripping is 0.01, the unintentional islanding probabilities would be 0.0567% (≥ 1 s), 0.0535% (≥ 2 s), and 0.0244% (≥ 3 s). Note that D²NDZ can also estimate NDZs considering the ride-through requirements based on the latest IEEE 1547 Standards. Such results are not included due to the limited space. Once the unintentional islanding frequencies are identified, further studies can be carried out either to reduce or even eliminate these frequencies, or to enable a stable system operation within NDZ, e.g., interactive control [30], proactive management [31], or adaptive optimization-based load shedding [32].

In summary, D²NDZ can produce results as close as those from EMT simulations, which enables fast offline or online assessment of the unintentional islanding of an arbitrary feeder. Before D²NDZ was adopted by Eversource Energy, it took an engineer up to a few months to build an NDZ for a specific feeder because this requires creating thousands of testing scenarios. With our D²NDZ tool, it only takes a few minutes to input data and generate results.

VI. CONCLUSION

A D²NDZ method is devised to evaluate the NDZs of distribution networks. Baseline NDZ is first derived in terms of the G/L and the power factor, and then the impact of DER dynamics are incorporated by augmenting the baseline NDZ to establish the overall NDZ. Further, a robust learning-based approach is introduced to determine D²NDZ's parameters through optimization. Numerical tests are performed on a large distribution feeder in Eversource Energy's service territory. Analyses and tests have confirmed the feasibility and effectiveness of D²NDZ. This paper also includes detailed investigations of the impacts of DER units and loads on NDZs.

A D²NDZ software package has recently been successfully deployed by Eversource Energy, where it is used as a practical, powerful, and efficient tool for planning, operating and protecting in distribution networks. As a data-driven, learning-based approach, D²NDZ can reduce utilities engineers case study time from months to just a few minutes, making it a promising tool for U.S. power utilities.

APPENDIX I LOAD ANALYSIS AFTER ISLANDING

Assume the load resistances before and after islanding can be expressed as follows.

$$R = R_I + R_P + R_C, \quad (45)$$

$$R + \Delta R = (R_I + \Delta R_I) + (R_P + \Delta R_P) + (R_C + \Delta R_C), \quad (46)$$

where R_I , R_P , R_C represent the real part of constant impedance, constant power and constant current loads before islanding, respectively; ΔR_I , ΔR_P , ΔR_C represent the incremental resistive portions in constant impedance, power and current loads after islanding.

TABLE IV
LINE IMPEDANCES BETWEEN NODES IN FIG. 4

From	To	$R(\Omega)$	$X(\Omega)$	From	To	$R(\Omega)$	$X(\Omega)$
1	2	0.001	0.001	2	3	0.004	0.014
3	4	0.008	0.031	4	5	0.048	0.177
5	44	0.005	0.011	67	68	0.005	0.011
44	45	0.002	0.005	45	46	0.002	0.005
46	47	0.147	0.337	47	48	0.415	0.558
65	66	0.005	0.012	48	49	0.004	0.006
49	50	0.004	0.006	50	51	0.070	0.094
51	52	0.013	0.017	52	53	0.278	0.373
53	59	0.012	0.002	59	60	0.055	0.011
60	61	0.002	0.002	61	62	0.001	0.001
62	63	0.001	0.001	63	64	0.001	0.001
53	54	0.286	0.385	54	55	0.014	0.018
55	56	0.095	0.219	56	57	0.004	0.010
57	58	0.293	0.671	5	6	0.033	0.120
6	7	0.003	0.013	7	8	0.012	0.043
8	9	0.060	0.138	9	10	0.020	0.046
10	11	0.061	0.140	11	12	0.003	0.007
12	13	0.003	0.007	13	14	0.285	0.654
79	80	0.006	0.014	14	15	0.165	0.381
15	16	0.168	0.384	16	81	0.006	0.013
82	83	0.005	0.013	81	84	0.003	0.007
84	85	0.003	0.006	85	86	0.355	0.815
86	87	0.003	0.006	87	88	0.003	0.006
88	89	0.030	0.006	16	17	0.171	0.393
17	18	0.007	0.016	18	19	0.296	0.582
19	20	0.002	0.004	20	21	0.049	0.113
21	22	0.046	0.171	21	92	0.007	0.009
92	95	0.007	0.009	95	96	0.007	0.009
92	93	0.003	0.004	93	94	0.003	0.004
22	23	0.003	0.013	23	24	0.002	0.006
24	25	0.002	0.006	97	98	0.004	0.015
25	26	0.002	0.006	26	27	0.163	0.603
27	28	0.016	0.057	28	29	0.239	0.883
29	30	0.002	0.006	30	31	0.002	0.006
77	78	0.003	0.012	31	32	0.056	0.129
32	33	0.006	0.015	33	34	0.309	0.709
34	69	0.024	0.054	73	74	0.005	0.013
69	70	0.003	0.006	70	71	0.014	0.007
71	72	3.650	1.917	34	35	0.036	0.082
35	36	0.171	0.090	36	37	0.634	0.591
37	38	0.043	0.016	75	76	0.003	0.004
38	39	0.043	0.017	39	40	0.569	0.219
40	41	0.029	0.011	41	42	0.006	0.018
42	43	0.002	0.003				

TABLE V
POWER LOADS AT EACH NODE IN FIG. 4

Node	P_n (kW)	Q_n (kVAR)	Node	P_n (kW)	Q_n (kVAR)
4	8.3	4.6	5	207.6	112.5
47	963.1	517.9	48	897.3	477.0
51	100.6	53.6	53	153.0	81.0
62	100.2	53.5	54	382.1	203.2
56	68.1	37.8	57	93.1	51.0
58	280.0	153.9	6	513.4	276.6
68	3.1	2.0	66	2.3	1.6
8	678.2	165.3	9	342.1	182.4
10	19.6	10.3	11	334.1	178.3
14	954.5	517.3	15	155.3	83.2
64	1.5	2.3	80	4.9	2.4
16	155.3	83.2	86	208.7	112.7
17	375.0	199.2	19	149.9	82.0
21	692.5	381.7	22	49.1	26.8
83	4.9	3.6	91	5.2	2.1
27	571.7	311.3	28	5.3	2.9
29	684.3	369.0	32	238.7	127.0
34	607.1	334.1	69	93.0	50.2
72	270.1	144.8	37	141.4	76.0
43	4.6	2.3	46	3.4	2.1

Given the percentages of constant impedance load, constant power load and constant current load, P_I , P_P , P_C the fractions between the corresponding resistances can be expressed as

$$R_I : R_P : R_C = P_P P_C : P_I P_C : P_I P_P. \quad (47)$$

Note that $\Delta R_I = 0$, and constant power and current loads should satisfy the following conditions:

$$\frac{V^2}{R_P} = \frac{(V + \Delta V)^2}{R_P + \Delta R_P}, \quad (48)$$

$$\frac{V}{R_C} = \frac{V + \Delta V}{R_C + \Delta R_C}. \quad (49)$$

Then ΔR_P and ΔR_C can be expressed as follows:

$$\Delta R_P = (2\mu + \mu^2) R_P = (2\mu + \mu^2) \frac{P_I}{P_P} R_I, \quad (50)$$

$$\Delta R_C = \mu R_C = \mu \frac{P_I}{P_C} R_I. \quad (51)$$

APPENDIX II DERIVATION OF (13)

In order to obtain (13)–(15) are substituted in (12). Detailed derivation is given as follows:

$$\begin{aligned} \left(\frac{Q_G}{P_L} \right)^S &= R \left(\frac{1}{2\pi f L} - 2\pi f C \right) - (1 + \mu)^2 R \cdot \\ &\quad \left(\frac{1}{2\pi(f + \Delta f)(L + \Delta L)} - 2\pi(f + \Delta f)(C + \Delta C) \right) \\ &= -(1 + \mu)^2 R \cdot \left(\frac{1}{2\pi f L (1 + \frac{\Delta L}{L} + \rho + \rho \frac{\Delta L}{L})} \right. \\ &\quad \left. - 2\pi f C \left(1 + \frac{\Delta C}{C} + \rho + \rho \frac{\Delta C}{C} \right) \right) \\ &= -(1 + \mu)^2 \cdot \left(\frac{Q_f}{(1 + \frac{\Delta L}{L}) (1 + \rho)} - Q_f \left(1 + \frac{\Delta C}{C} \right) \right. \\ &\quad \left. \cdot (1 + \rho) \right) \\ &= -(1 + \mu)^2 \cdot Q_f (1 + \rho) \cdot \left(\frac{1}{(1 + \frac{\Delta L}{L}) (1 + \rho)^2} - \left(1 + \frac{\Delta C}{C} \right) \right) \\ &\approx -(1 + \mu)^2 \cdot Q_f (1 + \rho) \cdot \left(\frac{1 - (1 + \frac{\Delta L}{L}) (1 + \frac{\Delta C}{C})}{(1 + \frac{\Delta L}{L})} \right) \\ &= (1 + \mu)^2 \cdot Q_f (1 + \rho) \cdot \left(\frac{\frac{\Delta L}{L} \frac{\Delta C}{C} + \frac{\Delta L}{L} + \frac{\Delta C}{C}}{(1 + \frac{\Delta L}{L})} \right). \quad (52) \end{aligned}$$

When $\Delta L \cdot \Delta C \approx 0$ and $1 + \frac{\Delta L}{L} \approx 1$, (13) can be obtained from (53).

APPENDIX III FREQUENCY ANALYSIS AFTER ISLANDING

The load resonant frequency before and after islanding can be expressed as follows.

$$f = \frac{1}{2\pi LC}, \quad (53)$$

$$f' = \frac{1}{2\pi(L + \Delta L)(C + \Delta C)}. \quad (54)$$

Thus the frequency deviation ρ can be given as follows.

$$\rho = \frac{f' - f}{f} = \frac{\sqrt{LC}}{\sqrt{(L + \Delta L)(C + \Delta C)}} - 1. \quad (55)$$

APPENDIX IV DETAILS OF THE DISTRIBUTION FEEDER IN FIG. 4

The line impedances between nodes in Fig. 4 are given in Table IV. And the power load at each node are summarized in Table V, Where P_n and Q_n are the total active power and reactive power at each node.

ACKNOWLEDGMENT

The authors would like to thank Emma Burris-Janssen for proofreading the manuscript. The authors also would like to thank the anonymous reviewers for the valuable comments.

REFERENCES

- [1] G. Pepermans, J. Driesen, D. Haeseldonckx, R. Belmans, and W. Dhaeseleer, "Distributed generation: Definition, benefits and issues," *Energy Policy*, vol. 33, no. 6, pp. 787–798, 2005.
- [2] Y. Li, P. Zhang, L. Zhang, and B. Wang, "Active synchronous detection of deception attacks in microgrid control systems," *IEEE Trans. Smart Grid*, vol. 8, no. 1, pp. 373–375, Jan. 2017.
- [3] T. Caldognetto, L. Dalla Santa, P. Magnone, and P. Mattavelli, "Power electronics based active load for unintentional islanding testbenches," *IEEE Trans. Ind. Appl.*, vol. 53, no. 4, pp. 3831–3839, Jul./Aug. 2017.
- [4] R. Walling, "Application of direct transfer trip for prevention of DG islanding," in *Proc. IEEE Power Energy Soc. Gen. Meeting*, 2011, pp. 1–3.
- [5] B. Bahrani, H. Karimi, and R. Iravani, "Nondetection zone assessment of an active islanding detection method and its experimental evaluation," *IEEE Trans. Power Del.*, vol. 26, no. 2, pp. 517–525, Apr. 2011.
- [6] H. Karimi, A. Yazdani, and R. Iravani, "Negative-sequence current injection for fast islanding detection of a distributed resource unit," *IEEE Trans. Power Electron.*, vol. 23, no. 1, pp. 298–307, Jan. 2008.
- [7] Z. Ye, A. Kolwalkar, Y. Zhang, P. Du, and R. Walling, "Evaluation of anti-islanding schemes based on nondetection zone concept," *IEEE Trans. Power Electron.*, vol. 19, no. 5, pp. 1171–1176, Sep. 2004.
- [8] D. Salles, W. Freitas, J. C. Vieira, and B. Venkatesh, "A practical method for nondetection zone estimation of passive anti-islanding schemes applied to synchronous distributed generators," *IEEE Trans. Power Del.*, vol. 30, no. 5, pp. 2066–2076, Oct. 2015.
- [9] M. E. Ropp, M. Begovic, A. Rohatgi, G. A. Kern, R. Bonn, and S. Gonzalez, "Determining the relative effectiveness of islanding detection methods using phase criteria and nondetection zones," *IEEE Trans. Energy Convers.*, vol. 15, no. 3, pp. 290–296, Sep. 2000.
- [10] L. A. Lopes and H. Sun, "Performance assessment of active frequency drifting islanding detection methods," *IEEE Trans. Energy Convers.*, vol. 21, no. 1, pp. 171–180, Mar. 2006.
- [11] Y. Jung, J. Choi, B. Yu, G. Yu, and J. So, "A novel active frequency drift method of islanding prevention for the grid-connected photovoltaic inverter," in *Proc. IEEE 36th Power Electron. Spec. Conf.*, 2005, pp. 1915–1921.
- [12] H. Vahedi and M. Karrari, "Adaptive fuzzy Sandia frequency-shift method for islanding protection of inverter-based distributed generation," *IEEE Trans. Power Del.*, vol. 28, no. 1, pp. 84–92, Jan. 2013.

- [13] S. Liu, S. Zhuang, Q. Xu, and J. Xiao, "Improved voltage shift islanding detection method for multi-inverter grid-connected photovoltaic systems," *IET Gener. Transmiss. Distrib.*, vol. 10, no. 13, pp. 3163–3169, 2016.
- [14] D. Reigosa, F. Briz, C. B. Charro, P. Garcia, and J. M. Guerrero, "Active islanding detection using high-frequency signal injection," *IEEE Trans. Ind. Appl.*, vol. 48, no. 5, pp. 1588–1597, Sep./Oct. 2012.
- [15] X. Wang, W. Freitas, V. Dinavahi, and W. Xu, "Investigation of positive feedback anti-islanding control for multiple inverter-based distributed generators," *IEEE Trans. Power Syst.*, vol. 24, no. 2, pp. 785–795, May 2009.
- [16] F.-J. Lin, Y.-S. Huang, K.-H. Tan, J.-H. Chiu, and Y.-R. Chang, "Active islanding detection method using d-axis disturbance signal injection with intelligent control," *IET Gen., Transmiss. Distrib.*, vol. 7, no. 5, pp. 537–550, 2013.
- [17] X. Chen and Y. Li, "An islanding detection algorithm for inverter-based distributed generation based on reactive power control," *IEEE Trans. Power Electron.*, vol. 29, no. 9, pp. 4672–4683, Sep. 2014.
- [18] W. K. Najy, H. Zeineldin, A. H. K. Alaboudy, and W. L. Woon, "A Bayesian passive islanding detection method for inverter-based distributed generation using esprit," *IEEE Trans. Power Del.*, vol. 26, no. 4, pp. 2687–2696, Oct. 2011.
- [19] F. De Mango, M. Liserre, and A. Dell'Aquila, "Overview of anti-islanding algorithms for PV systems. Part II: ActiveMethods," in *Proc. 12th Int. Power Electron. Motion Control Conf.*, 2006, pp. 1884–1889.
- [20] S. Samantaray, K. El-Arroudi, G. Joos, and I. Kamwa, "A fuzzy rule-based approach for islanding detection in distributed generation," *IEEE Trans. Power Del.*, vol. 25, no. 3, pp. 1427–1433, Jul. 2010.
- [21] N. Lidula and A. Rajapakse, "A pattern recognition approach for detecting power islands using transient signals—Part I: Design and implementation," *IEEE Trans. Power Del.*, vol. 25, no. 4, pp. 3070–3077, Oct. 2010.
- [22] G.-K. Hung, C.-C. Chang, and C.-L. Chen, "Automatic phase-shift method for islanding detection of grid-connected photovoltaic inverters," *IEEE Trans. Energy Convers.*, vol. 18, no. 1, pp. 169–173, Mar. 2003.
- [23] Y. Li *et al.*, "A generic method for the determination of non-detection zones in DER-dominated distribution grids," in *Proc. Power Energy Soc. Gen. Meeting*, 2018, pp. 1–5.
- [24] C. Wang, Y. Li, K. Peng, B. Hong, Z. Wu, and C. Sun, "Coordinated optimal design of inverter controllers in a micro-grid with multiple distributed generation units," *IEEE Trans. Power Syst.*, vol. 28, no. 3, pp. 2679–2687, Aug. 2013.
- [25] Y. Li, P. Zhang, and P. B. Luh, "Formal analysis of networked microgrids dynamics," *IEEE Trans. Power Syst.*, vol. 33, no. 3, pp. 3418–3427, May 2018.
- [26] Y. Low, J. E. Gonzalez, A. Kyrola, D. Bickson, C. E. Guestrin, and J. Hellerstein, "Graphlab: A new framework for parallel machine learning," unpublished paper, 2014. [Online]. Available: <https://arxiv.org/abs/1408.2041>
- [27] E. R. Sparks, A. Talwalkar, D. Haas, M. J. Franklin, M. I. Jordan, and T. Kraska, "Automating model search for large scale machine learning," in *Proc. 6th ACM Symp. Cloud Comput.*, 2015, pp. 368–380.
- [28] Y. Li and P. Zhang, "Unintentional islanding analysis for Eversource Energy feeders," Eversource Energy, Berlin, CT, USA, Tech. Rep., 2017.
- [29] *Interconnecting Distributed Resources with Electric Power Systems*, IEEE Standard 1547-2003, 2003.
- [30] Y. Zhang, L. Xie, and Q. Ding, "Interactive control of coupled microgrids for guaranteed system-wide small signal stability," *IEEE Trans. Smart Grid*, vol. 7, no. 2, pp. 1088–1096, Mar. 2016.
- [31] A. Gholami, T. Shekari, and S. Grijalva, "Proactive management of microgrids for resiliency enhancement: An adaptive robust approach," *IEEE Trans. Sustain. Energy*, 2017, to be published.
- [32] A. Gholami, T. Shekari, and A. Sun, "An adaptive optimization-based load shedding scheme in microgrids," in *Proc. 51st Hawaii Int. Conf. Syst. Sci.*, 2018.



Yan Li (S'13) received the B.Sc. and M.Sc. degrees in electrical engineering from Tianjin University, Tianjin, China, in 2008 and 2010, respectively. She is currently working toward the Ph.D. degree in electrical engineering with the University of Connecticut, Storrs, CT, USA. Her research interests include microgrids and networked microgrids, formal analysis, power system stability and control, software-defined networking, and cyber-physical security.



Peng Zhang (M'07– SM'10) received the Ph.D. degree in electrical engineering from the University of British Columbia, Vancouver, BC, Canada, in 2009. He is the Castleman Professor in engineering innovation and an Associate Professor of electrical engineering with the University of Connecticut, Storrs, CT, USA. He was a System Planning Engineer at BC Hydro and Power Authority, Vancouver. His research interests include microgrids, power system stability and control, cyber-physical security, and smart ocean systems. He is a registered Professional Engineer in British Columbia, Canada, and an individual member of CIGRÉ. He is an Editor for the IEEE TRANSACTIONS ON POWER SYSTEMS and the IEEE POWER AND ENERGY SOCIETY LETTERS.



Wenyuan Li (SM'89–F'02–LF'18) received the Ph.D. degree from Chongqing University, Chongqing, China, in 1987. He is a Professor with Chongqing University. He was with BC Hydro in Canada between 1991 and 2015. His research interests include smart grids, power system operation, planning, optimization and reliability assessment. He is a Fellow of the Canadian Academy of Engineering and a foreign member of the Chinese Academy of Engineering. He is a recipient of several IEEE Power and Energy Society (PES) Awards including the IEEE PES Roy Billinton Power System Reliability Award in 2011 and the IEEE Canada Electric Power Medal in 2014.



Joseph N. Debs received the B.Sc. degree in electrical engineering and the Master of Business Administration degree from the University of New Haven, West Haven, CT, USA, in 1986 and 1994, respectively. He is the Program Manager of Renewable Resources at Eversource Energy, Berlin, CT.



David A. Ferrante received the B.Sc. degree in civil engineering from the University of Vermont, Burlington, VT, USA, and the Master of Business Administration degree from the University of Hartford, West Hartford, CT, USA. He is the Manager of Distributed Energy Resources and Technology with Eversource Energy, Berlin, CT. Since 2008, he has been leading various corporate and public policy initiatives to integrate distributed energy resources and other advanced smart grid technologies that can integrate and interface with the electric power distribution systems. He and his team have integrated over 500 MWs of distributed energy resources such as photovoltaic generation, combined heat and power plant, fuel cells, microgrids, battery storage, and electric vehicle charging stations. He worked for more than 15 years in the natural gas industry for Yankee Gas Services Company as a Distribution Engineer, a Strategic Business Account Energy Consultant, and as a Director of customer service. He is certified by the American Gas Association as an Industrial Consultant. He is a Senior Member of the American Association of Energy Engineers and a registered Professional Engineer in the State of Connecticut.



Donald J. Kane received the B.S.E.E. and M.S. degrees in power systems management from the Worcester Polytechnic Institute, Worcester, MA, USA, in 1987 and 2013, respectively. He is a Lead Engineer with the Grid Modernization Group, Eversource Energy, Berlin, CT. He provides technical support for a variety of grid modernization efforts across Eversource. He has held engineering and supervisory roles in electric distribution planning/design, operations, and asset management, with a particular focus on distribution load flow modeling and analysis. He is a registered Professional Engineer in the State of Connecticut.



Samuel N. Woolard received the B.Sc. degree in electrical engineering from the University of Texas at Arlington, Arlington, TX, USA, in 2000, the M.E. degree in electrical engineering from the University of Idaho, Moscow, ID, USA, in 2006, and the Master of Business Administration degree from the University of Texas at Dallas, Dallas, TX, USA, in 2012. He has been the Director of Distribution Engineering with Eversource Energy, Berlin, CT, USA, since 2016. He was an Engineering Manager of Strategic Asset Management with Western Power and an Engineering Manager with Texas-New Mexico Power.



Roderick Kalbfleisch received the B.Sc. degree in mathematics from the Roberts Wesleyan College, Rochester, NY, USA, in 1986, the B.Sc. degree in electrical engineering from Clarkson University, Potsdam, NY, in 1987, and the M.Sc. degree in management and finance from the Rensselaer Polytechnic Institute, Troy, NY, in 2008. He is the Director of Substation Technical Engineering at Eversource Energy. He is leading the T&D Engineering team responsible for the electric system in Connecticut, Massachusetts and New Hampshire. This includes transmission and distribution substations across New England. He was the Director of T&D Substation Engineering, the Director of Systems Engineering, the Director of System Operations, and the Director of Meter Assets and Operations with Eversource Energy.



Kenneth B. Bowes received the B.Sc. degree in electrical engineering from the University of New Hampshire, Durham, NH, USA, and the M.Sc. degree in electrical engineering from the Rensselaer Polytechnic Institute, Troy, NY, USA.

He is the Vice President of Transmission Performance with Eversource Energy, Berlin, CT, USA. In that role, he is responsible for the leadership and direction of transmission performance as it relates to short- and long-term customer impacts and benefits, development of key siting witnesses, transmission performance indicators, Federal Energy Regulatory Commission and State Regulatory plans, and operational compliance. He serves as a technical consultant and expert witness for various regulatory proceedings and large transmission projects including Northern Pass Transmission and Bay State Wind. He has been part of the Eversource team for over 30 years, beginning in the System Test department. Since that time, he has held a variety of positions with increasing responsibility in the Engineering and Transmission areas, most recently serving as the Vice President of Engineering for Eversource's Connecticut Operations. In that previous role, he was responsible for all engineering activities for the electric distribution systems including distribution planning, distribution engineering and design, substation engineering, protection and control engineering, telecommunications engineering, and the geographic information systems for electric and gas operations. He established the reliability, asset management, and system resiliency strategies for a \$ 300 million annual program development and five-year capital program. He also managed the distributed generation, microgrid, new technology, and R&D activities for the company. Additionally, he executed the five-year \$ 450 million System Resiliency Program and the Stamford and Greenwich Infrastructure Improvement Projects. Under his leadership, Eversource received both the Emergency Recovery Award and the Emergency Assistance Award from the Edison Electric Institute in 2013.

Mr. Bowes is the past Chairman of the Edison Electric Institute's Transmission Committee and presently serves on the EEI Transmission and EEI Security Committees. He serves on the Board of Directors of Special Olympics Connecticut and the Bristol Boys and Girls Club. He is the Chairman of the Board of Nutmeg Big Brothers Big Sisters.



Andrew J. Kasznay (M'89) received the B.Sc. degree from Clarkson University, Potsdam, NY, USA, in 1989, and the M.Sc. degree from the Rensselaer Polytechnic Institute, Troy, NY, USA, in 1995, both in electrical engineering. He was a Manager of Asset and Strategy with Eversource Energy from 2010 to 2015. He is currently a Principal Engineer of Construction Operations with the United Illuminating Company, New Haven, CT, USA. He is a registered Professional Engineer in the States of Connecticut, Massachusetts, and Rhode Island.